


Folding model analyses of ^{12}C - ^{12}C and ^{16}O - ^{16}O elastic scattering using the density-dependent LOCV-averaged effective interaction

M. Rahmat and M. Modarres*

Department of Physics, University of Tehran, Tehran 143955961, Iran
 (Received 30 August 2017; revised manuscript received 7 February 2018; published 19 March 2018)

The averaged effective two-body interaction (AEI), which can be generated through the lowest order constrained variational (LOCV) method for symmetric nuclear matter (SNM) with the input [Reid68, *Ann. Phys.* **50**, 411 (1968)] nucleon-nucleon potential, is used as the effective nucleon-nucleon potential in the folding model to describe the heavy-ion (HI) elastic scattering cross sections. The elastic scattering cross sections of ^{12}C - ^{12}C and ^{16}O - ^{16}O systems are calculated in the above framework. The results are compared with the corresponding calculations coming from the fitting procedures with the input finite range *DDM3Y1*-Reid potential and the available experimental data at different incident energies. It is shown that a reasonable description of the elastic ^{12}C - ^{12}C and ^{16}O - ^{16}O scattering data at the low and medium energies can be obtained by using the above LOCV AEI, without any need to define a parametrized density-dependent function in the effective nucleon-nucleon potential, which is formally considered in the typical *DDM3Y1*-Reid interactions.

DOI: [10.1103/PhysRevC.97.034611](https://doi.org/10.1103/PhysRevC.97.034611)

I. INTRODUCTION

In recent years, there has been a growing interest in the heavy-ion (HI) scattering. These collision processes were investigated widely both experimentally and theoretically. One of the goals of studying the HI reactions is to determine the form of the most suitable effective nucleon-nucleon potential, to explain the experimental elastic scattering cross section data [1,2]. For many years, the use of empirical parametrization of nuclear potential was very common in the HI studies, but it is desirable to relate the nucleus-nucleus (\mathcal{NN}) interactions to the nucleon-nucleon (NN) nuclear potential [3]. Many attempts in this direction have been made, and recently, the double-folding (DF) model was extensively used by many groups in describing the HI scattering, since it gives a simple possibility of numerical handling in two nucleus scattering calculations [4].

In the folding model, the potential is usually generated by folding an effective NN interaction over the ground-state density distribution of the two nuclei [1,2]. In general, we need a well-defined effective NN interaction which reproduces the basic nuclear matter properties (like the saturation energy and density), and, on the other hand, it can be used as a basic input in the description of HI scattering qualitatively with respect to the experimental data [5]. The *M3Y* interaction [6] and its density-dependent versions [7–13], are usually used in the folding model. Recently the G -matrix and extended Hartree-Fock approaches [14–19], with and without the inclusion of the three body force (TBF) and the rearrangement term (RT), were applied for calculating the nucleon-nucleus and the nucleus-

nucleus scattering cross section calculations (but mainly at 70 MeV), as well as obtaining the nuclear matter saturation properties [equations of state (EOS)] [14]. The RT comes out in the case of calculating the single particle energy and the corresponding potential. But in the present work, we intend to apply the lowest order constrained variational averaged effective interaction LOCV AEI, which was generated by using the input Reid68 potential in our previous work [20], as the effective NN interaction, in the folding model to test the validity of our interaction in describing the HI elastic scattering. In this paper, we limit ourselves to the elastic scattering of spherical projectile and spherical target nuclei, so we consider the ^{12}C - ^{12}C and ^{16}O - ^{16}O elastic scattering.

A brief discussion about the LOCV method is given in the Appendix. Contrary to the G -matrix approach, in the LOCV formalism (which is based on the cluster expansion [21]), the wave functions, e.g., the correlation functions, are calculated through the Euler-Lagrange differential equations, whereas the application of G operator on the plane wave generates the interacting wave functions. Another advantage of the cluster expansion is its expansion in the powers of correlation functions (in the G -matrix language the wound parameter) and the first power of the NN potential. So it converges faster than the G -matrix approach which is an expansion in the powers of the potential. On the other hand since we directly calculate the LOCV AEI, there is no need to calculate the RT in our approach. In Table I, the results of the LOCV saturation properties of the symmetrical nuclear matter (SNM) calculation for the Reid68 and Δ -Reid68 potentials (in comparison to the empirical one) are presented. The LOCV method is self-consistently predicted for the EOS of SNM (for details see the Appendix and Table V). The one-body (E_1 , simply the Fermi energy), two-body (E_2), and three-body

*Corresponding author: mmodares@ut.ac.ir

TABLE I. The nuclear matter saturation parameters (for Reid and Δ -Reid potentials) extracted from Ref. [22] (E_3 denotes the inclusion of the three-body cluster energy; see the Appendix).

	With Reid		With Δ -Reid		Empirical
	$E_1 + E_2$	$E_1 + E_2 + E_3$	$E_1 + E_2$	$E_1 + E_2 + E_3$	
Saturation Fermi momentum (fm $^{-1}$)	1.61	1.46	1.55	1.44	1.38
Saturation binding energy (MeV)	22.54	21.85	16.28	15.52	15.86
Compressibility (MeV)	340	298	300	277	(200–300)
Convergence parameter	0.127	0.085	0.093	0.062	

cluster (E_3) terms as well as the convergence parameters are discussed in the Appendix.

In some of our LOCV calculations, we have taken into account the effects of TBF such as the Δ box diagram (see the Appendix). But in the present work, since we intend to compare our results with those coming from the $M3Y$ interaction [6], which is based on the Reid68 potential, our results will be limited to this interaction. However we hope in our future works that the other interactions as well as the effects of the TBF on the nucleus-nucleus differential cross sections will be evaluated. In Table V it is clearly demonstrated that the LOCV method predicts the SNM saturation properties close to other methods, even with or without TBF [22]. We should point out here that there are no extra parameters and conditions on the LOCV method to predict the saturation properties of SNM.

In our recent paper [20], we derived the averaged effective two-body interactions (AEI) through the lowest order constrained variational (LOCV) calculations for the SNM with the Reid68 [23], the Δ -Reid68 [24] [which takes into the account the effect of three-body force (TBF)], and the $A\nu_{18}$ [25] interactions as the input phenomenological nucleon-nucleon potentials, and reformulated them in the radial and density-dependent parts as well as its direct and exchange components. Note that the radial parts are fixed and density-dependent functions only depend on density which becomes a constant at fixed density, i.e., similar to the $M3Y$ calculations. Here as we stated above, we only use the LOCV AEI with the input Reid68 potential in the folding model and compare our results with those coming from the $DDM3Y1$ -Reid which uses a finite range potential as the direct and exchange components, i.e., $M3Y$ interactions [4]. The LOCV effective two-body interactions were tested by calculating the properties of the light and heavy closed shell nuclei [26–28], and recently it was used to calculate the in-medium nn cross section, the transport properties of neutron matter [29,30], and the normal liquid helium-3 [31]. In these works, it was shown that the LOCV AEI gave reasonable results in comparison to the corresponding available data.

This article is organized as follows: In Sec. II, we briefly review the theoretical formalism of the double folding model. The density distributions and the different kinds of effective interactions used in the folding model as well as the computational procedure are also discussed in this section. The results of the calculations and discussions are given in Sec. III, and Sec. IV is devoted to the summary and conclusions.

II. THEORETICAL FORMALISM

A. Double folding model

Satchler and Love [32] presented the basic idea of the folding model in detail and in Ref. [4] an improved version of the folding model was introduced to calculate the exchange part of the HI potential. We give here only a brief description of this model and refer the reader to Refs. [1,2,32–35] for details. In the first order of Feshbach's theory for the optical potential, the microscopic nucleus-nucleus potential can be evaluated as an antisymmetrized Hartree-Fock type potential for the dinuclear system [1,2,4]:

$$U = U_D + U_{EX} = \sum_{i \in A_1, j \in A_2} [\langle ij | \nu_D | ij \rangle - \langle ij | \nu_{EX} | ji \rangle], \quad (1)$$

where $|i\rangle$ and $|j\rangle$ refer to the single-particle wave functions of nucleons in the two colliding nuclei A_1 and A_2 , respectively; ν_D and ν_{EX} are the direct and exchange parts of the effective NN interaction. After doing some algebra, one can explicitly write the energy-dependent direct and exchange potentials as

$$U_D(E, \mathbf{R}) = \int d\mathbf{r}_p d\mathbf{r}_t \rho_p(\mathbf{r}_p) \rho_t(\mathbf{r}_t) \nu_D(\rho, E, s),$$

$$\mathbf{s} = \mathbf{r}_p - \mathbf{r}_t + \mathbf{R}, \quad (2)$$

$$U_{EX}(E, \mathbf{R}) = \int d\mathbf{r}_p d\mathbf{r}_t \rho_p(\mathbf{r}_p; \mathbf{r}_p + \mathbf{s}) \rho_t(\mathbf{r}_t; \mathbf{r}_t - \mathbf{s})$$

$$\times \nu_{EX}(\rho, E, s) e^{i\mathbf{k}_{rel} \cdot \mathbf{s} / A_{red}}. \quad (3)$$

Note that, in general, the one-body density is written as $\rho(\mathbf{r}, \mathbf{r}')$. In the case of direct term, it becomes $\rho(\mathbf{r}_p)$ or $\rho(\mathbf{r}_t)$, i.e., the diagonal terms, where \mathbf{r}_p and \mathbf{r}_t are the positions of the two nucleons in the nuclei p (projectile) and t (target), respectively, $\mathbf{s} = \mathbf{r}_p - \mathbf{r}_t + \mathbf{R}$ corresponds to the distance between the two specified interacting points of the projectile and the target, and \mathbf{R} is a vector from the center of the t nucleus to that of the p nucleus. But in the case of the exchange terms, we have $\rho(\mathbf{r}, \mathbf{r}')$ for each nucleus, i.e., nondiagonal terms, with $(\mathbf{r} = \mathbf{r}_p, \mathbf{r}' = \mathbf{r}_p + \mathbf{s})$ or $(\mathbf{r} = \mathbf{r}_t, \mathbf{r}' = \mathbf{r}_t - \mathbf{s})$. So for the exchange term the densities are the functions of two different coordinates [4]. In the above equations, the wave number \mathbf{k}_{rel} is associated with the relative motion of colliding nuclei, which is given by

$$k_{rel}^2(\mathbf{R}) = 2m_n A_{red} [E_{c.m.} - U(E, \mathbf{R}) - V_C(\mathbf{R})] / \hbar^2, \quad (4)$$

where $A_{red} = A_p A_t / (A_p + A_t)$, m_n , $E_{c.m.}$ and E are the reduced mass number, the bare nucleon mass, the center-of-mass (c.m.) energy, and the incident laboratory energy per nucleon, respectively. Here $U(E, \mathbf{R}) = U_D(E, \mathbf{R}) + U_{EX}(E, \mathbf{R})$ and $V_C(\mathbf{R})$ are the total nuclear and the Coulomb potentials, respectively. It can be seen from Eq. (3) that the energy-dependent HI potential is nonlocal through its exchange term. For simplicity of the numeric calculations, a realistic local expression for the density matrix is usually used [36]:

$$\rho(\mathbf{R}, \mathbf{R} + \mathbf{s}) \simeq \rho\left(\mathbf{R} + \frac{\mathbf{s}}{2}\right) \hat{j}_1\left[k_F\left(\mathbf{R} + \frac{\mathbf{s}}{2}\right)s\right], \quad (5)$$

where $\hat{j}_1(x) = 3(\sin x - x \cos x)/x^3$. The explicit form of $k_F(\mathbf{R})$ is given in Ref. [4]. In order to specify the overlap density during the HI collision, we have applied the procedure used in Ref. [4] that is called frozen density approximation (FDA). In this approach, the overlap density ρ is taken to be the sum of the densities of the target and the projectile densities at the midpoint of the internucleon separation, i.e.,

$$\rho = \rho_p\left(\mathbf{r}_p + \frac{\mathbf{s}}{2}\right) + \rho_t\left(\mathbf{r}_t - \frac{\mathbf{s}}{2}\right). \quad (6)$$

This procedure simply corresponds to the local density approximation assumed in the different nuclear matter studies [4, 26–28].

After performing some transformations one can obtain the exchange potential in the following local form:

$$\begin{aligned} U_{EX}(E, \mathbf{R}) &= 4\pi \int_0^\infty v_{EX}(s, E) s^2 ds \hat{j}_0[k(\mathbf{R})s/M] \int f_1(\mathbf{r}, s) \\ &\quad \times f_2(\mathbf{r} - \mathbf{R}, s) F[\rho_p(\mathbf{r}) + \rho_t(\mathbf{r} - \mathbf{R})] d\mathbf{r}, \end{aligned} \quad (7)$$

where $[F(\rho)]$ will be defined later on; i.e., see Eqs. (19)–(25) in Sec. II B]

$$f_{1(2)}(\mathbf{r}, s) = \rho_{p(t)}(r) \hat{j}_1[k_{F1(2)}(r)s], \quad \hat{j}_0(x) = \frac{\sin x}{x}. \quad (8)$$

Applying the folding formulas in the momentum space [36], one can write the exchange potential as

$$U_{EX}(E, \mathbf{R}) = 4\pi \int_0^\infty G(\mathbf{R}, s) \hat{j}_0[k(\mathbf{R})s/M] v_{EX}(s, E) s^2 ds. \quad (9)$$

The explicit form of the $G(\mathbf{R}, s)$ function can be found in Ref. [4].

As it can be seen from Eq. (4), the wave number of relative motion $k_{rel}(R)$ depends on the total HI potential, so we encounter a self-consistency problem in obtaining the exchange part of the HI potential at each radial point. In general, this problem can be overcome by applying an iterative procedure, as performed for the first time by Chaudhuri *et al.* [37]. However, in Refs. [34, 35] a closed expression was used to obtain the exchange potential by using the multiplication theorem of the Bessel function $\hat{j}_0[k(\mathbf{R})s/M]$. In this paper, we use the iterative method to ensure the self-consistency at all the radial points, in which we chose $U_D(E, R)$ as the starting potential to enter in the $\hat{j}_0[k(\mathbf{R})s/M]$ term in the exchange integral, Eq. (9).

Since the effective NN interactions applied in the folding model are real, the calculated HI potentials are also real, so the imaginary part of the HI potential is usually treated phenomenologically and its parameters are adjusted to optimize the fit to the observed scattering. In most cases, the Woods-Saxon (WS) shape (with volume or the surface type) is used for the imaginary potential. Finally the HI potential can be written in the general form as

$$\begin{aligned} U(E, R) &= N_R [U_D(E, R) + U_{EX}(E, R)] \\ &\quad - i W_V \left[1 + \exp\left(\frac{R - R_V}{a_V}\right) \right]^{-1} \\ &\quad + 4i W_D a_D \frac{d}{dR} \left[1 + \exp\left(\frac{R - R_D}{a_D}\right) \right]^{-1}, \end{aligned} \quad (10)$$

where the renormalization coefficient N_R together with the parameters of the imaginary potential are adjusted to give the best fit to the scattering data. The renormalization coefficient N_R is needed to account roughly for the many-nucleon exchange effects and the dynamical polarization potential (ΔU) [32]. The volume or surface WS terms (the second and the third terms at above formula) are usually used as the imaginary potential in the elastic scattering analysis. However, we only use the volume term in our present calculations.

In the calculation of the exchange potential, we need also the Coulomb potential $V_C(R)$. According to Ref. [38], the different models for the Coulomb potential do not have a serious effect on the theoretical predictions. So, in our optical model (OM) calculations, we chose the Coulomb potential to be a simple interaction between a point charge and a uniform one with the radius R_C [3],

$$V_C(R) = Z_p Z_t e^2 \begin{cases} \frac{1}{R} & R > R_C \\ \frac{1}{2R_C} \left[3 - \left(\frac{R}{R_C}\right)^2 \right] & R < R_C \end{cases} \quad (11)$$

with $e^2 = 1.44 \text{ MeV fm}$ and $R_C = R_p + R_t$, $R_i = 1.76 Z_i^{1/3} - 0.96 \text{ fm}$, with $i = p, t$.

B. Choice of the effective interaction and the density distribution

As it can be seen from Eqs. (2) and (3), the basic inputs in the folding model are the nuclear densities of the colliding nuclei in their ground state and the effective NN interaction. The density distributions should be normalized as

$$\int \rho_i(\mathbf{r}_i) d\mathbf{r}_i = A_i, \quad (12)$$

where A_i is the mass number of the projectile or the target nucleus. In this paper, the nuclear densities of two colliding nuclei are approximated by the two-parameter Fermi distribution: $\rho(r) = \rho_0 \{1 + \exp[(r - c)/a]\}^{-1}$ with parameters taken from Table 1 of Ref. [39].

Given correct nuclear densities as inputs for the folding calculations, it is still necessary to have an appropriate NN interaction for a reasonable prediction of the nucleus-nucleus potential. The bare nucleon-nucleon interaction, obtained from analysis of NN scattering measurements, is too strong to be used directly in the folding model, so it is common to

use an effective in-medium interaction [1,2]. To evaluate an in-medium NN interaction starting from a realistic free NN interaction still remains a challenge for the nuclear many-body theory. Therefore, most of the microscopic nuclear reaction calculations so far still use different kinds of effective in-medium NN interaction [4]. One of the most popular choices for the NN interactions was based on the $M3Y$ interactions and its density-dependent versions [7–13]. These interactions are designed to reproduce the G -matrix elements of the Reid [6] and Paris [40] NN interactions in an oscillator basis [1,26–28]. We refer to these as the $M3Y$ -Reid and the $M3Y$ -Paris interactions, respectively. The explicit forms for the direct part of interactions are [1,2]

$$M3Y\text{-Reid: } v_D(r) = \left[7999 \frac{e^{-4r}}{4r} - 2134 \frac{e^{-2.5r}}{2.5r} \right] \text{ MeV,} \quad (13)$$

$$M3Y\text{-Paris: } v_D(r) = \left[11\,062 \frac{e^{-4r}}{4r} - 2538 \frac{e^{-2.5r}}{2.5r} \right] \text{ MeV,} \quad (14)$$

whereas the exchange parts of interactions in the finite-range exchange (FRE) form ($M3Y$ /FRE) are written as [1–4]

$$M3Y\text{-Reid: } v_{EX}(r) = \left[4631 \frac{e^{-4r}}{4r} - 1787 \frac{e^{-2.5r}}{2.5r} - 7.847 \frac{e^{-0.7072r}}{0.7072r} \right] \text{ MeV,} \quad (15)$$

$$M3Y\text{-Paris: } v_{EX}(r) = \left[-1524 \frac{e^{-4r}}{4r} - 518.8 \frac{e^{-2.5r}}{2.5r} - 7.847 \frac{e^{-0.7072r}}{0.7072r} \right] \text{ MeV.} \quad (16)$$

However, in many other calculations, the zero-range pseudopotential ($M3Y/PP$) is used to represent the knock-on exchange [1,2]. But in this work we focus on the finite range interactions, i.e., Eqs. (13) and (15).

The older potentials based upon the density-independent $M3Y$ interactions could reasonably reproduce the data of HI scattering at the forward angle, or low energies [1,2]. Also, the ground-state energy of nuclear matter (in a

standard Hartree-Fock calculation) using the $M3Y$ interactions is calculated in Ref. [7]. One can realize that the density-independent $M3Y$ interactions do not fulfill the saturation condition for cold nuclear matter, i.e., leading to collapse. To ensure the predication of the nuclear matter saturation, an appropriate density-dependent factor is introduced into the original $M3Y$ interaction. It is usually taken as an independent factor that multiplied to the original radial $M3Y$ interaction, i.e., $v_{D(EX)}(r, \rho) = F(\rho)v_{D(EX)}(r)$. As it is stated in Refs. [1,2], there is no theoretical justification for this factorization, but it leads to improving the description of nuclear matter properties and the HI scattering data. Various forms for $F(\rho)$ were proposed. In the $DDM3Y1$ and $CDM3Yn$ ($n = 1-6$), the following is assumed for the density-dependent form of the potential:

$$F(\rho) = C[1 + \alpha \exp(-\beta\rho) - \gamma\rho]. \quad (17)$$

In $BDM3Yn$ ($n = 0-3$) interactions, a power law dependent on ρ is supposed:

$$F(\rho) = C(1 - \alpha\rho^\beta). \quad (18)$$

The parameters C , α , β , and γ are adjusted to reproduce the saturation of cold symmetric nuclear matter at $\rho_0 = 0.17 \text{ fm}^{-3}$ and a binding energy per nucleon of about 16 MeV. The values of these parameters for $CDM3Yn$, $DDM3Y1$, and $BDM3Yn$ interactions are given in Refs. [1,2,7,38,41]. As we pointed out before for comparison we focus on the finite range $DDM3Y1$ interaction [4].

In the course of these application to the \mathcal{NN} scattering data, it is necessary to introduce an additional energy dependent factor over which is provided by localization of the exchange potential

$$v_{D(EX)}^{M3Y}(r, \rho, E) = v_{D(EX)}^{M3Y}(r)F(\rho)g(E), \quad (19)$$

where $g(E) = [1 - k(E/A)]$ with $k = 0.002 \text{ MeV}^{-1}$ or $k = 0.003 \text{ MeV}^{-1}$ for the Reid interaction or the Paris interaction [3], respectively. However none of the above potentials come from a Hamiltonian based many-body microscopic calculation.

In the present work, the LOCV density-dependent averaged effective two-body interaction (AEI) is generated though the LOCV method with the bare nucleon-nucleon phenomenological Reid68 potential, and inserted as an input to the folding model calculations. In our previous work [20], we obtained the direct and the exchange parts of the density-dependent nucleon-nucleon AEI as follows (see the Appendix for the definition of a and \mathcal{V}):

$$\bar{\mathcal{V}}_{\text{eff}}^D(r, \rho) = \frac{\sum_{\alpha, i, j, k} (2T+1)(2J+1) \frac{1}{2} \mathcal{V}_\alpha^{j, k}(r, \rho) a_\alpha^{(i)^2}(r, \rho)}{\sum_{\alpha, i} (2T+1)(2J+1) \frac{1}{2} a_\alpha^{(i)^2}(r, \rho)}, \quad (20)$$

$$\bar{\mathcal{V}}_{\text{eff}}^{EX}(r, \rho) = \frac{\sum_{\alpha, i, j, k} (2T+1)(2J+1) \frac{1}{2} [(-1)^{L+S+T}] \mathcal{V}_\alpha^{j, k}(r, \rho) a_\alpha^{(i)^2}(r, \rho)}{\sum_{\alpha, i} (2T+1)(2J+1) \frac{1}{2} [(-1)^{L+S+T}] a_\alpha^{(i)^2}(r, \rho)}, \quad (21)$$

where $\alpha = JLS T$; J is the total orbital angular momentum of two nucleons, i.e., L plus S , and T is the total isospin of two nucleons. Then we have reformulated these interactions as the product of a pure radial and a pure density-dependent part:

$$\bar{\mathcal{V}}_{\text{eff}}^{D(EX)}(r, \rho) = \bar{\mathcal{V}}^{D(EX)}(r) F^{D(EX)}(\rho). \quad (22)$$

TABLE II. The parameters of the density-dependent part of the direct and the exchange components [$F^{D(EX)}(\rho)$] of the LOCV AEI using the Reid68 interaction as the input potentials.

	\mathcal{C}	α	β
Direct component	0.38	5.03	3.22
Exchange component	13.57	-0.9	0.12

Here, we chose $\bar{V}^{D(EX)}(r)$ and $F^{D(EX)}(\rho)$ to give the best fit to the LOCV $\bar{V}_{\text{eff}}^{D(EX)}(r, \rho)$ and the corresponding equation of state (LOCV-EOS) of nuclear matter. The reader should note that, by this statement, we mean that the fitted potentials should again reproduce the SNM saturation properties given in Table I.

There are many different functions which can fit $F^{D(EX)}(\rho)$ well enough. A detailed role of description of density-dependent factor (F) can be found in our previous work [20], where we stated that the LOCV AEI includes a radial part and a density-dependent part and we show that the radial part form of the LOCV AEI is fixed in any density (exactly like the $M3Y$ type interactions) and the EOS of SNM without taking into account the density-dependent factor did not fulfill the saturation condition and the system was collapsed (see Fig. 7 of Ref. [20]). But one should notice that our density-dependent factor is not an external factor and it comes from the LOCV calculations. So, we just parametrized it in a suitable form [i.e., see below, Eq. (23)] (the exponential dependent form for density). In Ref. [21], we compared the direct and exchange parts of the LOCV AEI with the corresponding results of the $M3Y$ interactions (see Figs. 1 and 4 of Ref. [20]).

So as we stated above, similar to our previous work [20], in order to reproduce the LOCV-EOS of nuclear matter properly, we use the power-law dependent on ρ : $F^{D(EX)}(\rho) = \mathcal{C}^{D(EX)}(1 - \alpha^{D(EX)}\rho^{\beta^{D(EX)}})$. In this paper, we use the exponential dependent form for ρ (similar to the $DDM3Y1$ interaction):

$$F^{D(EX)}(\rho) = \mathcal{C}^{D(EX)}[1 + \alpha^{D(EX)} \exp(-\beta^{D(EX)}\rho)]. \quad (23)$$

This choice allows us to easily calculate the integration of the double-folding equations in the momentum space [1,2]. The parameters of Eq. (23) are given in Table II.

Similar to the $M3Y$ interactions, in order to apply the LOCV AEI to the \mathcal{NN} scattering data, we need to add an explicit energy-dependent factor to our LOCV AEI to obtain the best description of HI scattering by taking into account the variation in the incident energy. We found that this factor can be assumed as the linear dependent to the incident energy per nucleon, which is similar to the $M3Y$ interactions, i.e., $g(E) = [1 - k(E/A)]$. So, we can rewrite the LOCV AEI as

$$\bar{V}_{\text{eff}}^{D(EX)}(r, \rho, E) = \bar{V}^{D(EX)}(r)F^{D(EX)}(\rho)g(E). \quad (24)$$

Here, as in other HI works, the k is chosen to give the best fit to the \mathcal{NN} scattering data. It is shown that in the case of our LOCV AEI by choosing $k = 0.003 \text{ MeV}^{-1}$, the optimized fit

will be acquired. However, the calculation is not very sensitive to this parameter if it is chosen in its order.

C. Computational procedure

At first, we calculate the real part of the folded potential for ^{12}C - ^{12}C and ^{16}O - ^{16}O elastic scattering by the double folding formula, i.e., Eqs. (2) and (3). Then we use the LOCV AEI as the effective NN interactions and the two-parameter Fermi distribution for the nuclear densities of the projectile and the target nuclei. Now, in order to compute the scattering differential cross section, we also use the FRESKO code developed by Thompson [42] which is developed for the calculation of different types of nucleon-nucleus and nucleus-nucleus scattering cross sections. This code is capable of using our folded potential directly, to calculate the elastic scattering cross section.

We will discuss our resulting potentials and the elastic scattering cross section for ^{12}C - ^{12}C and ^{16}O - ^{16}O systems in the next section. Generally, the goodness of our resulting cross section is quantified via the χ^2 expression [1,2],

$$\chi^2 = \frac{1}{N_\sigma} \sum_{i=1}^{N_\sigma} \frac{(\sigma_{th} - \sigma_{ex})^2}{(\Delta\sigma_{ex})^2}, \quad (25)$$

where σ_{th} and σ_{ex} are the theoretical and the experimental cross sections and $\Delta\sigma_{ex}$ is defined as the uncertainties in the experimental cross sections, respectively. N_σ is the total number of angles at which measurements are made.

III. RESULTS AND DISCUSSIONS

As it was pointed out in the previous section, in order to calculate the direct and exchange components of the real part of the HI optical potential, we use the direct and exchange parts of the LOCV AEI as the effective NN potential in the double folding formula [Eqs. (2) and (3)]. Since the wave number of relative motion $k_{\text{rel}}(R)$, Eq. (4), depends on the total HI potential, we are faced with a self-consistency problem in obtaining the exchange part of the HI potential at each radial point. So, we apply the iterative method at each point and use $U_D(E, R)$ as the starting potential to enter $\hat{j}_0(k(\mathbf{R})_s/M)$ in the exchange integral, Eq. (9), i.e., as it is performed when one considers the $M3Y$ interactions in the folding formula [4].

Unfortunately at small internuclear distances ($R \leq 1 \text{ fm}$), the iterative method for calculating the exchange potential based on the LOCV AEI does not converge reasonably. Of course, with increasing the incident energy, this problem will be solved. Due to this low convergence speed of iterative method in the case of the insertion of the LOCV AEI in the folding formula, we need a much higher number of iterations with respect to the $M3Y$ interactions in obtaining the exact self-consistent results for $U_{EX}(E, R)$, especially at small internuclear distances. According to Ref. [4], in the case of the $M3Y$ interactions, the number of iterations required is around 20 at the smallest radii and ranges from 3 to 5 at the surface region, while, in the case of the LOCV AEI, it is around 150–200 at the smallest radii and around 2 or 3 at the surface region. For this reason, too much CPU computer time is needed to calculate the exchange part of the HI potential in the case of

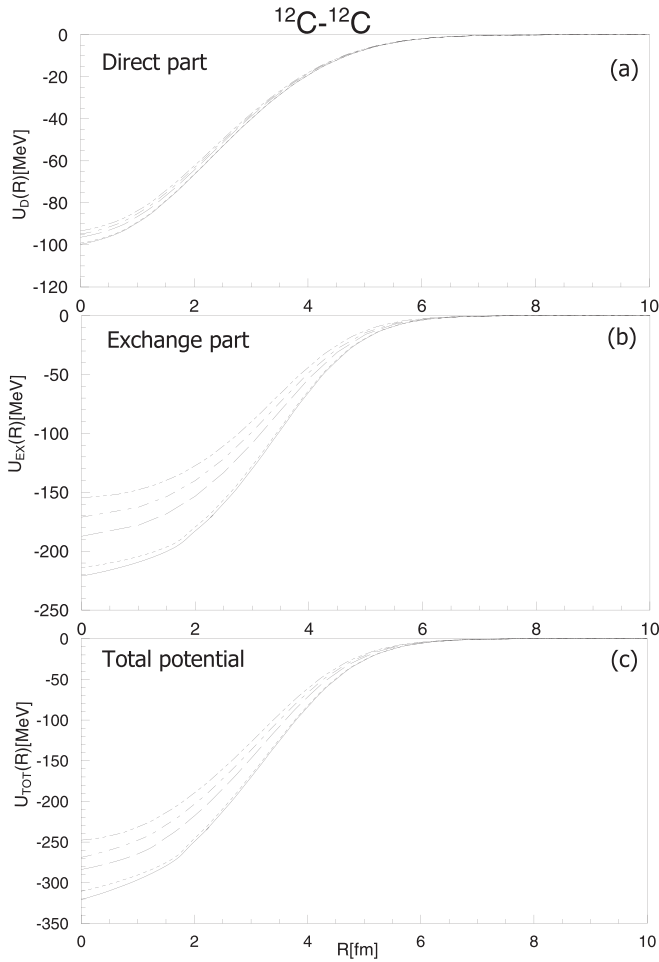


FIG. 1. The calculated direct and the exchange components and the total folded potential, by using LOCV AEI for the $^{12}\text{C}-^{12}\text{C}$ system at the several incident energies, i.e., $E_{\text{lab}} = 112$ (full curve), 126.7 (short-dash curve), 240 (long-dash curve), 300 (long-short-dash curve), 360 (long-double-short-dash curve) MeV.

the LOCV AEI. For example for the $^{12}\text{C}-^{12}\text{C}$ elastic scattering at $E_{\text{lab}} = 300$ MeV, it took about 50 h computer CPU time by using the high performance computing (HPC) machine of the university of Tehran. Because of the different radial shapes of the LOCV AEI with respect to the $M3Y$ interactions at the small distances, this problem is expected. Conversely to the $M3Y$ potentials, due to short range correlations coming from the channel-dependent correlation functions, at very small distances, the direct and exchange components of the LOCV AEI go to zero (see Figs. 1–4 of Ref. [20]) and this behavior makes the iterative method not converge at these distances as quickly as for the $M3Y$ interactions. While, the $M3Y$ interactions are constructed from the selected channels of, for example, the Reid68 potential, i.e., the singlet and the triplet even and odd components, one is not faced with this problem.

In Figs. 1 and 2, we plot the calculated direct, exchange, and also the total components of the folded potential by using the LOCV AEI for $^{12}\text{C}-^{12}\text{C}$ and $^{16}\text{O}-^{16}\text{O}$ systems at several incident energies, i.e., 112, 126.7, 240, 300, and 360 MeV for $^{12}\text{C}-^{12}\text{C}$ and 124, 145, 250, 350, and 480 MeV in the case

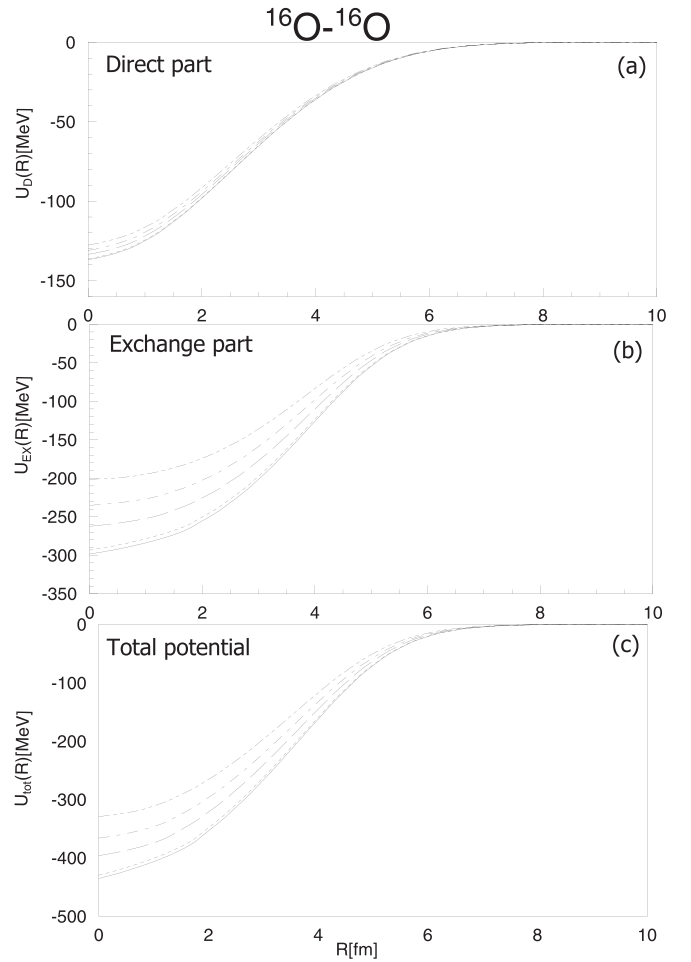


FIG. 2. As in Fig. 1 but for the $^{16}\text{O}-^{16}\text{O}$ system and $E_{\text{lab}} = 124$ (full curve), 145 (short-dash curve), 250 (long-dash curve), 350 (long-short-dash curve), 480 (long-double-short-dash curve) MeV.

of $^{16}\text{O}-^{16}\text{O}$ [note that we extrapolate the folded potential at the small distances ($R < 1$ fm) for some points that in the iterative method do not converge rapidly for the calculation of the exchange potential based on LOCV AEI]. Comparing the exchange parts with the direct parts at each incident energy, one can observe that most of the energy dependence of the HI potential arises from the exchange part, as one should expect. We also notice that at small internuclear distances, which correspond to large overlap densities ($\rho > \rho_0$), the exchange potential is deeper than the direct potential, especially at lower energies, and this shows that the density-dependent contribution of the HI potential predominately comes from the exchange term. On the other hand, in the surface region, which corresponds to the small overlap densities, all the calculated direct and exchange potentials are close in strength and slope. Figures 1 and 2 also show that with increasing the incident energy of the projectile, the depth of the HI potential at the origin is decreased systematically. Similar results were already reported in calculating the folded potential using the $M3Y$ interactions; see, for example, Refs. [4,5].

We compare our calculated folded potential using the LOCV AEI with the corresponding results of $DDM3Y1$ [4]

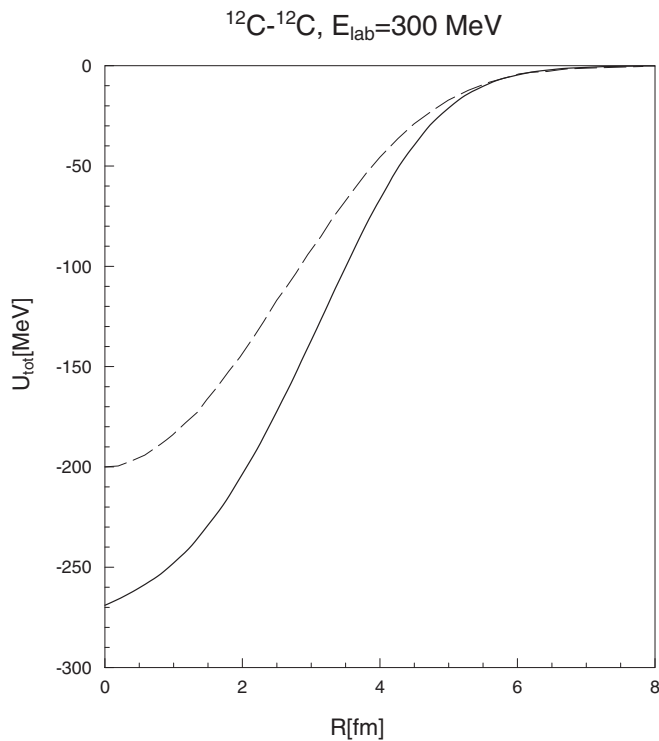


FIG. 3. The comparison of the calculated folded potentials using the LOCV AEI (the full curve) and the *DDM3Y1* [4] (short-dash curve) potential for the ^{12}C - ^{12}C scattering at $E_{\text{lab}} = 300$ MeV.

for the cases of ^{12}C - ^{12}C at $E_{\text{lab}} = 300$ MeV and ^{12}O - ^{12}O at $E_{\text{lab}} = 350$ MeV in Figs. 3 and 4, respectively. It can be observed that the folded potentials by using the LOCV AEI are deeper than the *DDM3Y1* ones. For the other energies, the similar results are obtained.

The results of our folding analysis for ^{12}C - ^{12}C elastic scattering at incident energies ranging from 112 to 360 MeV with the FRESKO code are presented in Fig. 5 while Table III shows the WS parameters of the imaginary part of the HI potential for the same system and at the same energies as well as σ_R and χ^2 (with respect to the experimental data, see the next paragraph). In this paper we take the imaginary part of the HI potential as the conventional WS form and adjust its parameters to obtain the best description of the experimental scattering data in the whole angular range at each incident energy. The parameters in Table III are close to those found in

TABLE III. The WS parameters of the imaginary part of HI potential used in our folding analysis of the ^{12}C - ^{12}C elastic scattering at $E_{\text{lab}} = 112, 126.7, 240, 300, 360$ MeV.

E_{lab} (MeV)	N_R	W_V (MeV)	R_V (fm)	a_V (fm)	σ_R (mb)	χ^2
112	0.9383	17.4	5.403	0.70	1526.79	36.52
126.7	0.9230	19.10	5.128	0.79	1563.51	41.86
240	1.0207	28.90	5.266	0.69	1551.95	39.34
300	0.9731	33.82	4.991	0.72	1497.85	18.33
360	0.9684	34.5	4.808	0.70	1374.73	9.81

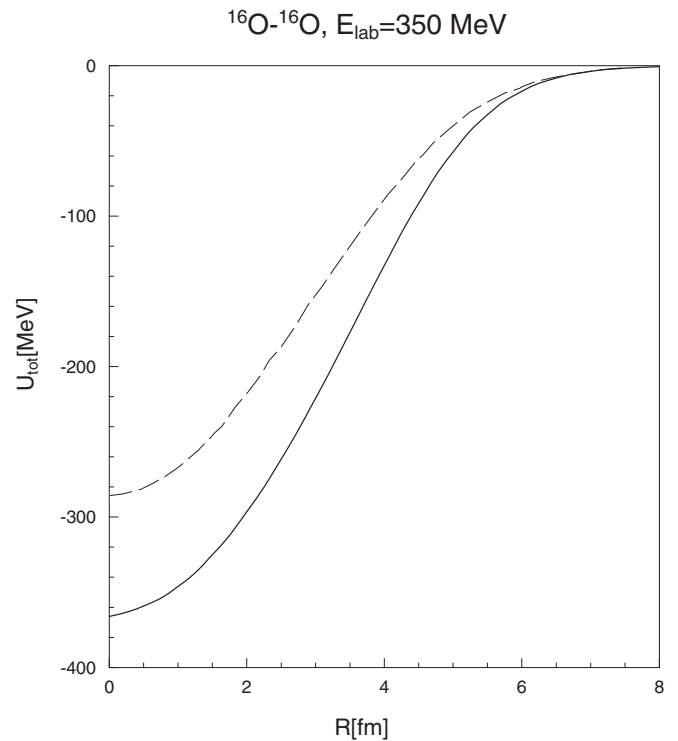


FIG. 4. As in Fig. 3 but for the ^{16}O - ^{16}O scattering at $E_{\text{lab}} = 350$ MeV.

an earlier analysis for *DDM3Y1*-Reid (see Table 2 of Ref. [4]). Table III also shows that the best fit to the scattering data can be found by using the values of N_R which are slightly deviated from unity. This result indicates that the high-order effects are negligible in our calculations.

Figures 5(a)–5(e) show the calculated cross section of ^{12}C - ^{12}C elastic scattering at several incident energies, i.e., 112, 126.7, 240, 300, and 360 MeV, by using the LOCV AEI folded potential in the FRESKO code. The scattering experimental data [43–51] and the resulting cross sections of the *DDM3Y1* [4] are also presented. It is observed that a quite good description of data scattering can be obtained by using the LOCV AEI and adjusting the imaginary potential parameters and renormalization coefficient. However, in comparison to the *DDM3Y1* (Reid) results [4], our results may not be too satisfactory, especially at forward angles, but one should notice that the *DDM3Y1* potential was constructed from the selected channels of the Reid68 potential and its density-dependent factor was added to it later, to provide a reasonable description of HI scattering data and the equation of state (EOS) of nuclear matter, while the LOCV AEI are constructed based on the many-body calculations without any free parameters in the LOCV calculations and its density-dependent part comes directly from the LOCV formalism (obviously the LOCV formalism has its own EOS, i.e., LOCV EOS). It is worthwhile to say that, by increasing the incident energy, a better fit to the scattering data is achieved using the LOCV AEI at forward angles.

The calculated cross sections using the LOCV AEI for ^{16}O - ^{16}O elastic scattering at incident energies ranging from

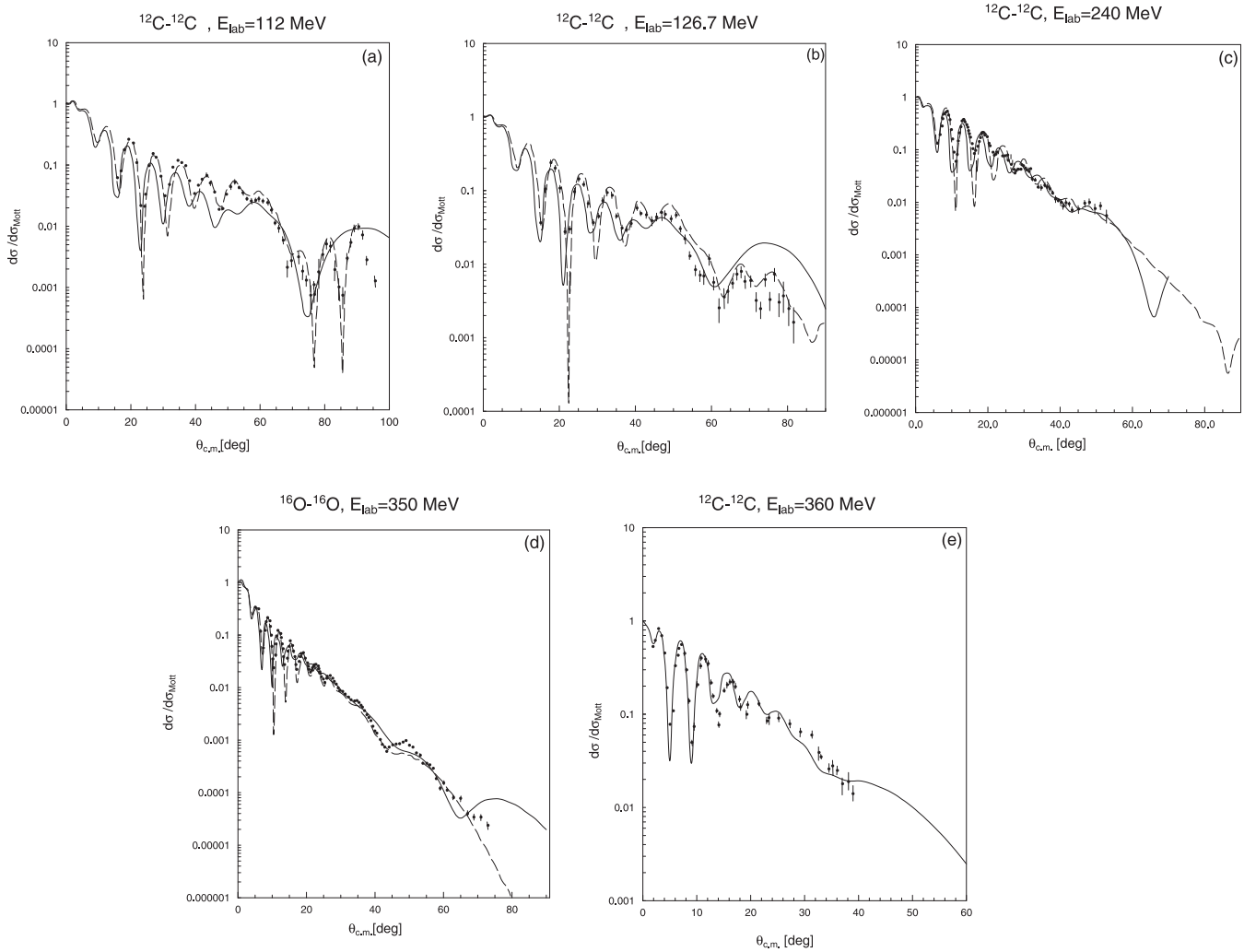


FIG. 5. The calculated cross sections of the $^{12}\text{C}-^{12}\text{C}$ elastic scattering at $E_{\text{lab}} = 112, 126.7, 240, 300, 360$ MeV by using the LOCV AEI (the full curve) using the FRESKO code. The experimental scattering data (the full dotted points) and the resulting cross section of the finite range interaction *DDM3Y1* [4] (the dash curve) are also presented. The experimental data are taken from Refs. [43–46].

124 to 480 MeV are plotted in Figs. 6(a)–6(e). The scattering experimental data [43–51] show a clear refractive pattern at large angles and a diffractive pattern produced by an interference between near-side and far-side components of the scattering amplitude at the small angles. The refractive pattern can be clearly distinguished from the diffractive structure, i.e., it shifts substantially towards the small angles with increasing incident energy [5].

One can realize that our calculated cross sections can predict reasonably the behavior of scattering data on large ranges of scattering angles [43–51]. Similar to the results obtained above for the $^{12}\text{C}-^{12}\text{C}$ system, there exist considerable differences between our results with respect to the experimental data and those coming from *DDM3Y1*. Again, a similar discussion can be made for these results as the one we made above for ^{12}C . In this case, it can also be observed that the agreement of our calculations with the scattering data are getting better as the energies of projectile are increased. To improve the agreement of the calculated cross sections using the *DDM3Y1-Reid*

and *DDM3Y1-Paris* with data in the large-angle region, in Refs. [4,5] a surface (WSD) term was included in the imaginary part of the potential. We hope, in our future works, we could investigate the inclusion of the WSD term to improve our results.

Table IV shows the parameters of our WS imaginary potential and renormalization coefficient for the $^{16}\text{O}-^{16}\text{O}$ system

TABLE IV. The same as Table III but for the $^{16}\text{O}-^{16}\text{O}$ elastic scattering at $E_{\text{lab}} = 124, 145, 250, 350, 480$ MeV.

E_{lab} (MeV)	N_R	W_V (MeV)	R_V (fm)	a_V (fm)	σ_R (mb)	χ^2
124	0.9455	15.3	6.30	0.93	2201.99	34.34
145	1.007	16.4	6.199	0.95	2226.17	37.07
250	1.011	31.6	5.695	0.86	2091.89	39.71
350	0.9890	36.76	5.544	0.77	1876.58	21.19
480	0.9703	42.65	5.241	0.79	1778.03	42.37

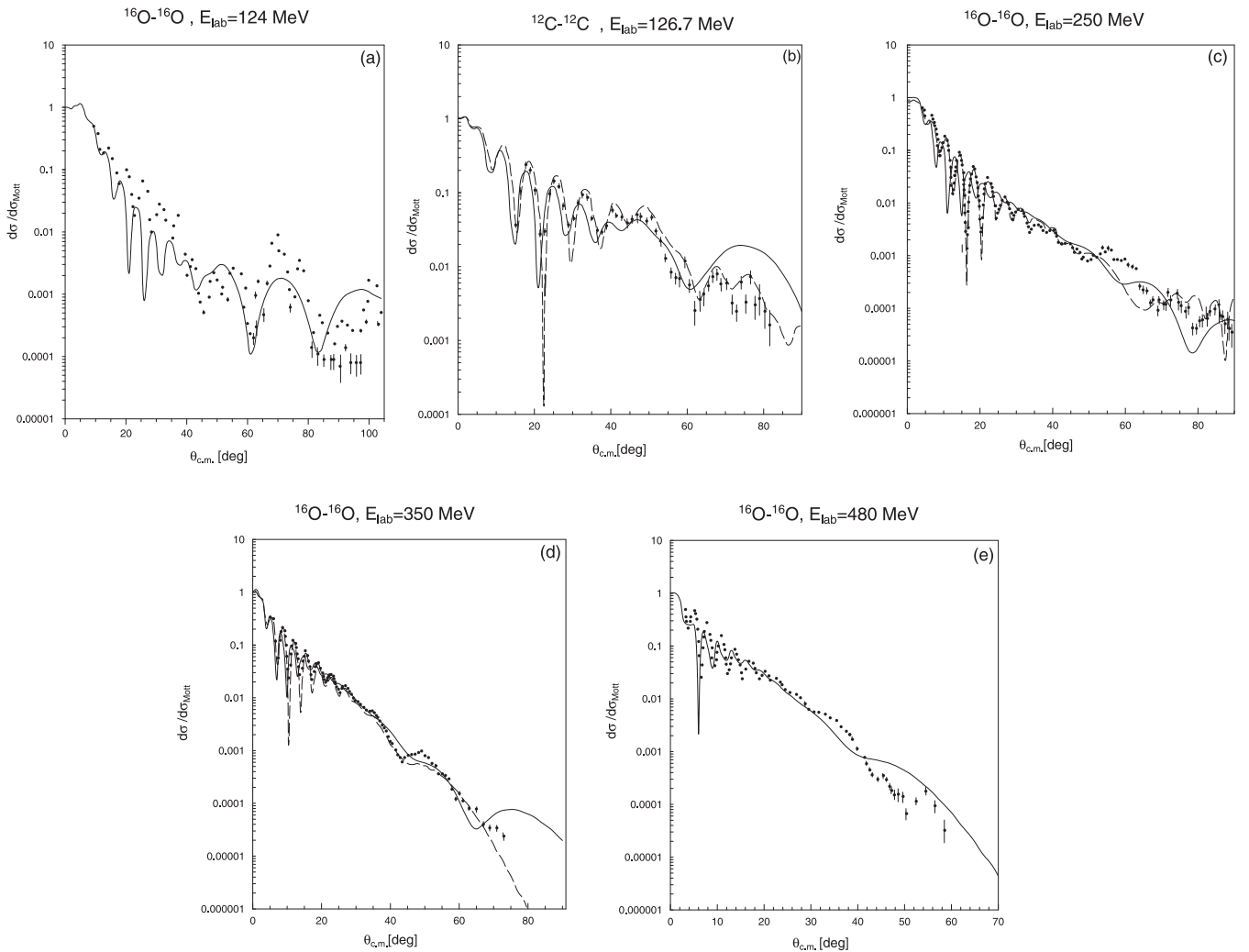


FIG. 6. As in Fig. 5 but for the ^{16}O - ^{16}O scattering at $E_{\text{lab}} = 124, 145, 250, 350, 480$ MeV. The experimental scattering data are taken from Refs. [47–51].

at different incident energies, as above. Again, we can see that the values of N_R are close to unity and our WS parameters are in agreement to the WS parameters of *DDM3Y1* analysis [4].

IV. SUMMARY

In conclusion, we analyzed the experimental data of ^{12}C - ^{12}C and ^{16}O - ^{16}O elastic scattering at different incident energies, within the standard optical model (OM), using the density-dependent LOCV AEI. The direct and exchange parts of LOCV AEI were generated based on the LOCV method for the symmetric nuclear matter, using the Reid68 interaction as the input phenomenological potential. In order to use our interaction in the folding model, we separated the radial and the density-dependent parts of the LOCV AEI. Our calculated cross sections for the ^{12}C and ^{16}O systems indicate that a quite reasonable description of data scattering can be obtained by using the LOCV AEI and adjusting the imaginary potential parameters and the renormalization coefficient. Our calculations favor a rather weak imaginary potential and a small deviation

of the renormalization factor from unity. Comparing our calculations with corresponding results of the *DDM3Y1*, we show some considerable differences. But one should notice that the *M3Y* interactions are semiphenomenological potentials and they are constructed from the selected channels of the Reid potential, i.e., the singlet and triplet even and odd components and the parameters of its density-dependent part are adjusted to gain a reasonable description of HI scattering data and the EOS of nuclear matter. So, it is natural to fit the scattering data better than ours. While the LOCV AEI are based on the many-body calculation with the phenomenological *NN* potential without any free parameters, i.e., there are no free parameters in the LOCV formalism besides the *NN* potential and its density-dependent part comes directly from the self-consistent LOCV calculations. So it is meaningful to apply the LOCV AEI interaction to the heavy-ion scattering as the first attempt, but we hope improvement of the present model could be achieved in the near future.

The spite of the slow convergence speed of iterative procedure in using the LOCV AEI in calculating the exchange potential, especially at small internuclear distances which

increases the computing time, since the LOCV AEI are based on the many-body calculations, they are more trustable for the \mathcal{NN} collision calculations. So, with respect to the above arguments, because the LOCV AEI provides a reasonable description of the normal nuclear matter [20] as well as the HI elastic scattering data simultaneously, we can claim the LOCV AEI is a good candidate to approximate the NN interaction for the nuclear matter and finite nuclei.

Finally we should note that the insertion of other phenomenological nucleon-nucleon potential, such as the A_{v18} potential, should not make any dramatic change to our present results, but it is worthwhile to investigate.

ACKNOWLEDGMENTS

The authors would like to acknowledge the Research Council of University of Tehran and the Iran National Science Foundation (INSF) for the grants provided to them. They also would like to sincerely thank Prof. I. Thompson for his valuable help regarding the FRESKO code.

APPENDIX A: A BRIEF INTRODUCTION TO THE LOCV FORMALISM WITH THE REID68 INTERACTION

In the LOCV method, we use an ideal Fermi gas type wave function for the single particle states and the variational techniques to find the wave function of the interacting system [22,52–56], i.e.,

$$\psi = \mathcal{F}\Phi, \quad (\text{A1})$$

where (\mathcal{S} is a symmetrizing operator)

$$\mathcal{F} = \mathcal{S} \prod_{i>j} F(ij). \quad (\text{A2})$$

The correlation functions $F(ij)$ are operators and they are written as

$$F(ij) = \sum_{\alpha,k} f_{\alpha}^{(k)}(ij) O_{\alpha}^{(k)}(ij). \quad (\text{A3})$$

In the above equation $\alpha = \{S, L, J, T\}$, $k = 1, 3$ and

$$O_{\alpha}^{k=1,4} = 1, \left(\frac{2}{3} + \frac{1}{6}S_{12}\right)^I, \left(\frac{1}{3} - \frac{1}{6}S_{12}\right)^I. \quad (\text{A4})$$

In the case of the Reid68 potential, the spin-singlet channels with the orbital angular momentum $L \neq 0$ and the spin-triplet channels with $L \neq J \pm 1$, k is superfluous and set only to unity, while for $L = J \pm 1$ it takes the values of 2 and 3. All of the channel correlation functions $f_{\alpha}^{(1)}$, $f_{\alpha}^{(2)}$, and $f_{\alpha}^{(3)}$ heal to the modified Pauli function $f_P(r)$,

$$f_P(r) = [1 - l(k_F r)^2]^{-1/2} \quad (\text{A5})$$

with

$$l(x) = \frac{3}{2x} \mathcal{J}_1(x), \quad (\text{A6})$$

where $\mathcal{J}_J(x)$ are the familiar spherical Bessel functions and the Fermi momenta k_F is fixed by the nuclear matter density, i.e., $k_F = (\frac{3\pi^2}{2}\rho)^{1/3}$.

The nuclear matter energy per nucleon is [22,53–56],

$$E_{in} = T_F + E_{MB}[F]. \quad (\text{A7})$$

T_F is simply the Fermi gas kinetic energy and it is written as

$$T_F = \frac{3}{5} \frac{\hbar^2 k_F^2}{2m}. \quad (\text{A8})$$

The many-body energy term $E_{MB}[F]$ is calculated by constructing a cluster expansion for the expectation value of our Hamiltonian,

$$H = \sum_i \frac{p_i^2}{2m} + \sum_{i>j} V_{ij}, \quad (\text{A9})$$

where V_{ij} is the bare N - N interaction. Then, we keep only the first two terms in a cluster expansion of the energy functional:

$$\begin{aligned} E[F] &= \frac{1}{A} \frac{\langle \Psi | H | \Psi \rangle}{\langle \Psi | \Psi \rangle} \\ &= T_F + E_{MB} = T_F + E_2 + E_3 + \dots \end{aligned} \quad (\text{A10})$$

The two-body energy term is defined as

$$E_2 = (2A)^{-1} \sum_{ij} \langle ij | \mathcal{V}(12) | ij \rangle_a, \quad (\text{A11})$$

where

$$\mathcal{V}(12) = -\frac{\hbar^2}{2m} [F(12), [\nabla_{12}^2, F(12)]] + F(12)V(12)F(12) \quad (\text{A12})$$

and the two-body antisymmetrized matrix element $\langle ij | \mathcal{V} | ij \rangle_a$ are taken with respect to the single-particle functions composing Φ , i.e., the plane waves. In the LOCV formalism E_{MB} is approximated by E_2 and one hopes that the normalization constraint makes the cluster expansion converge very rapidly and bring the many-body effect into the E_2 term.

By inserting a complete set of two-particle states twice in Eq. (A11) and performing some algebra, we can rewrite the two-body term as follows:

$$E_2 = E_c^{NN} + E_{\mathcal{T}}^{NN}, \quad (\text{A13})$$

where (c and \mathcal{T} stand for the central and tensor parts, respectively)

$$\begin{aligned} E_i^j &= \frac{2}{\pi^4 \rho} \sum_{\alpha} (2T+1)(2J+1) \frac{1}{2} \{1 - (-1)^{L+S+T}\} \\ &\times \int_0^{\infty} r^2 dr \mathcal{V}_{\alpha}^{i,j}(r, \rho) a_{\alpha}^{(1)^2}(r) \end{aligned} \quad (\text{A14})$$

and ($i = c$ and \mathcal{T})

$$\mathcal{V}_\alpha^{c,NN}(r,\rho) = \frac{\hbar^2}{m} \left\{ f_\alpha^{(1)^2} + \frac{m}{\hbar^2} V_\alpha^c f_\alpha^{(1)^2} \right\}, \quad (\text{A15})$$

$$\begin{aligned} \mathcal{V}_\alpha^{\mathcal{T},NN}(r,\rho) = & \left\{ \frac{\hbar^2}{m} \left\{ f_\alpha^{(2)^2} + \frac{m}{\hbar^2} (V_\alpha^c + 2V_\alpha^\mathcal{T} - V_\alpha^{LS}) f_\alpha^{(2)^2} \right\} a_\alpha(r)^{(2)^2} + \frac{\hbar^2}{m} \left\{ f_\alpha^{(3)^2} + \frac{m}{\hbar^2} (V_\alpha^c - 4V_\alpha^\mathcal{T} - 2V_\alpha^{LS}) f_\alpha^{(3)^2} \right\} a_\alpha^{(3)^2}(r) \right. \\ & \left. + \left\{ r^{-2} (f_\alpha^{(2)^2} - f_\alpha^{(3)^2} + \frac{m}{\hbar^2} V_\alpha^{LS} f_\alpha^{(2)} f_\alpha^{(3)}) \right\} b_\alpha^2 \right\} a_\alpha^{(1)^{-2}}(r), \end{aligned} \quad (\text{A16})$$

$$a_\alpha^{(1)^2}(r,\rho) = I_J(r,\rho), \quad (\text{A17})$$

$$a_\alpha^{(2)^2}(r,\rho) = (2J+1)^{-1} [(J+1)I_{J-1}(r,\rho) + JI_{J+1}(r,\rho)], \quad (\text{A18})$$

$$a_\alpha^{(3)^2}(r,\rho) = (2J+1)^{-1} [JI_{J-1}(r,\rho) + (J+1)I_{J+1}(r,\rho)], \quad (\text{A19})$$

$$b_\alpha^2(r,\rho) = 2J(J+1)(2J+1)^{-1} [I_{J-1}(r,\rho) - I_{J+1}(r,\rho)], \quad (\text{A20})$$

$$I_J(r,\rho) = (2\pi^6 \rho^2)^{-1} \int_{|\mathbf{k}_1|, |\mathbf{k}_2| \leq k_F} d\mathbf{k}_1 d\mathbf{k}_2 \mathcal{J}_J^2(|\mathbf{k}_1 - \mathbf{k}_2|r). \quad (\text{A21})$$

The potential functions $V_\alpha^c, V_\alpha^\mathcal{T}, \dots$, etc., are given in Refs. [26,27]. The calculation of E_3 is discussed in Ref. [57] and references therein.

The normalization constraint as well as the coupled and uncoupled differential equations for the NN channels, coming from the Euler-Lagrange equations, are similar to those described in Refs. [22,53–56].

The following are important points consider in the LOCV formalism: (i) Besides the interparticle potentials, no free parameter is used in the LOCV method, i.e., it is fully self-consistent. (ii) To keep the higher cluster terms as small as possible, it considers the constraint in the form of a normalization condition [22,53–56]. This was tested by calculating the three-body cluster terms with both the state-averaged and the state-dependent correlation functions [57]. (iii) In order to perform an exact functional minimization of the two-body cluster energy with respect to the short-range behavior of correlation functions, it assumes a particular form for the long-range part of the correlation functions. (iv) Rather than simply parametrizing the short-range behavior of the correlation functions, it performs an exact functional minimization [58]. So, in this respect it also saves an enormous amount of computational time. For example, a nuclear matter LOCV calculation with the Nijmegen group potentials at the given density takes a few minutes of CPU time on a 1.8-GHz personal computer.

Recently [59], it was shown that the neutron (nuclear) matter LOCV calculations with the various two-body interactions, e.g., the Bethe homework potential and the Argonne Av_8^{\prime} interaction [58], reasonably agree with those of FHNC and auxiliary field diffusion Monte Carlo (AFDMC) [60–65] methods. Moreover, it was realized that the different many-body methods such as the LOCV and the fermion hypernetted chain FHNC approaches give results close to each other when

the normalization constraint is imposed in its correct form. Therefore, the normalization constraint plays an important role in minimizing the many-body terms.

So in the LOCV framework by using, e.g., the Reid68 interaction, we solve the set of Euler-Lagrange differential equations to find the correlation functions. Then we can find the SNM-EOS by calculating the expectation value of the Hamiltonian. The minimization of the LOCV EOS gives some values for the binding and saturation density of the SNM, demonstrated in Tables I and V. Obviously, as is well known, one should not expect to get the exact SNM empirical values. But in the $M3Y$ type interactions, the situation is different; in order to ensure the empirical saturation density and the binding energy as well as incompressibility of the symmetric nuclear matter, an external density-dependent factor is multiplied to the original radial $M3Y$ interactions and the constants of this density-dependent function are obtained such that one could reproduce these empirical saturation properties for the SNM. So the case of the LOCV method is different from the $M3Y$ type interactions. The separation of radial and density-dependent parts of the LOCV AEI is done only to make it possible to use the LOCV AEI in the double folding procedure.

In Table V we compare the LOCV results on the saturation properties of SNM by using different interactions with other many-body techniques (the BB, BHF, CBF, and BHF-ESC stand for the Brueckner-Bethe, Brueckner-Hartree-Fock, correlated-basis function, and BHF using extended-soft-core interactions; see Refs. [22] and [14], and references therein, for details, respectively). So the EOS of SNM is directly calculated by the LOCV formalism and there is no other constraint for obtaining the saturation properties of SNM.

Finally we should mention that the effect of TBFs have been fully discussed especially in Refs. [22,53,55].

TABLE V. Saturation energy and the density of nuclear matter as well as its incompressibility for different potentials and many-body methods. See Ref. [22] for details.

Potential	Method	Author	ρ_0 (fm $^{-3}$)	$E(\rho_0)$ (MeV)	\mathcal{K} (MeV)
AV_{18}	LOCV	BM [22]	0.310	-18.46	302
AV_{14}	LOCV	BM [22]	0.290	-15.99	248
	FHNC	WFF [22]	0.319	-15.60	205
	BB	DW [22]	0.280	-17.80	247
	BHF	BBB [22]	0.256	-18.26	
UV_{14}	LOCV	BM [22]	0.366	-21.20	311
	FHNC	CP [22]	0.349	-20.00	
	FHNC	WFF [22]	0.326	-17.10	243
$UV_{14} + \text{TBF}$	LOCV	BM [22]	0.170	-17.33	276
	FHNC	WFF [22]	0.157	-16.60	261
	CBF	FFP [22]	0.163	-18.30	269
Δ -Reid	LOCV	MI [22]	0.258	-16.28	300
Reid	LOCV	OBI [22]	0.294	-22.83	340
	LOCV	MO [22]	0.230	-14.58	238
ESC	BHF	FSY [14]	~ 0.14	~ -12.00	~ 84
ESC-TBA	BHF	FSY [14]	~ 0.16	~ -14.00	~ 173
ESC-TBA-strong	BHF	FSY [14]	~ 0.19	~ -16.00	~ 260
Empirical			0.170	-15.86	(200–300)

- [1] M. E. Brandan and G. R. Satchler, *Phys. Rep.* **285**, 143 (1997).
[2] K. Amos, P. J. Dortmans, H. V. von Geramb, S. Karataglidis, *Adv. Nucl. Phys.* **25**, 275 (2000).
[3] G. L. Zhang, H. Liu, and X. Y. Le, *Chin. Phys. B* **18**, 5385 (2009).
[4] D. T. Khoa, W. von Oertzen, and H. G. Bohlen, *Phys. Rev. C* **49**, 1652 (1994).
[5] D. T. Khoa, W. von Oertzen, H.G. Bohlen, G. Bartnitzky, H. Clement, Y. Sugiyama, B. Gebauer, A. N. Ostrowski, T. Wilpert, M. Wilpert, and C. Langner, *Phys. Rev. Lett.* **74**, 34 (1995).
[6] G. Bertsch, J. Borysowicz, H. McManus, and W. G. Love, *Nucl. Phys. A* **284**, 399 (1977).
[7] D. T. Khoa and W. von Oertzen, *Phys. Lett. B* **304**, 8 (1993).
[8] D. T. Khoa and W. von Oertzen, *Phys. Lett. B* **342**, 6 (1995).
[9] D. T. Khoa, W. von Oertzen, and A. A. Ogloblin, *Nucl. Phys. A* **602**, 98 (1996).
[10] D. T. Khoa, G. R. Satchler, and W. von Oertzen, *Phys. Rev. C* **56**, 954 (1997).
[11] D. T. Khoa, H. S. Than, and D. C. Cuong, *Phys. Rev. C* **76**, 014603 (2007).
[12] D. N. Basu, P. Roy Chowdhury, C. Samanta, *Nucl. Phys. A* **811**, 140 (2008).
[13] P. Roy Chowdhury, C. Samanta, and D. N. Basu, *Phys. Rev. C* **80**, 011305 (2009).
[14] T. Furumoto, Y. Sakuragi, and Y. Yamamoto, *Phys. Rev. C* **78**, 044610 (2008).
[15] S. Rafi, M. Sharma, D. Pachouri, W. Haider, and Y. K. Gambhir, *Phys. Rev. C* **87**, 014003 (2013).
[16] M. Toyokawa, M. Yahiro, T. Matsumoto, K. Minomo, K. Ogata, and M. Kohno, *Phys. Rev. C* **92**, 024618 (2015).
[17] T. Furumoto, Y. Sakuragi, and Y. Yamamoto, *Phys. Rev. C* **80**, 044614 (2009).
[18] K. Minomo, M. Toyokawa, M. Kohno, and M. Yahiro, *Phys. Rev. C* **90**, 051601 (2014).
[19] D. T. Khoa, N. H. Phuc, D. T. Loan, and B. M. Loc, *Phys. Rev. C* **94**, 034612 (2016).
[20] M. Modarres and M. Rahmat, *Nucl. Phys. A* **934**, 148 (2015).
[21] J. W. Clark, *Prog. Part. Nucl. Phys.* **2**, 89 (1979).
[22] G. H. Bordbar and M. Modarres, *J. Phys. G: Nucl. Part. Phys.* **23**, 1631 (1997).
[23] R. V. Reid, *Ann. Phys.* **50**, 411 (1968).
[24] A. M. Green, J. A. Niskanen, and M. E. Sainio, *J. Phys. G, Nucl. Part. Phys.* **4**, 1055 (1978).
[25] R. B. Wiringa, V. G. J. Stoks, and R. Schiavilla, *Phys. Rev. C* **51**, 38 (1995).
[26] M. Modarres and N. Rasekhinejad, *Phys. Rev. C* **72**, 014301 (2005).
[27] M. Modarres and N. Rasekhinejad, *Phys. Rev. C* **72**, 064306 (2005).
[28] M. Modarres and H. Mariji, *Nucl. Phys. A* **859**, 16 (2011).
[29] M. Modarres and M. Rahmat, *Nucl. Phys. A* **903**, 40 (2013).
[30] M. Modarres and M. Rahmat, *Nucl. Phys. A* **921**, 19 (2014).
[31] M. Modarres and M. Rahmat, *Physica A* **466**, 396 (2017).
[32] G. R. Satchler and W. G. Love, *Phys. Rep.* **55**, 183 (1979).
[33] D. T. Khoa, A. Faessler, and N. Ohtsuka, *J. Phys. G: Nucl. Part. Phys.* **16**, 1253 (1990).
[34] D. T. Khoa, *Nucl. Phys. A* **484**, 376 (1988).
[35] D. T. Khoa and O. M. Knyazkov, *Z. Phys. A: At. Nucl.* **328**, 67 (1987).
[36] X. Csmispnd and A. Bouyssy, *Phys. Lett. B* **73**, 263 (1978).
[37] A. K. Chsudhuri, D. N. Bssu, and B. Sinhs, *Nucl. Phys. A* **439**, 415 (1985).
[38] R. M. DeVries and M. R. Clover, *Nucl. Phys. A* **243**, 528 (1975).
[39] M. El-Azab Farid and G. R. Satchler, *Nucl. Phys. A* **438**, 525 (1985).
[40] N. Anantaraman, N. H. Toki, and G. F. Bertsch, *Nucl. Phys. A* **398**, 269 (1983).
[41] I. I. Gontchar, D. J. Hinde, M. Dasgupta, and J. O. Newton, *Phys. Rev. C* **69**, 024610 (2004).
[42] I. Thompson, www.fresco.org.uk.

- [43] R. G. Stokstad, R. M. Wieland, G. R. Satchler, C. B. Fulmer, D. C. Hensley, S. Raman, L. D. Rickertsen, A. H. Snell, and P. H. Stelson, *Phys. Rev. C* **20**, 655 (1979).
- [44] H. G. Bohlen, X. S. Chen, J. G. Cramer, P. Frobrich, B. Gebauer, H. Lettau, A. Miczaika, W. von Oertzen, R. Ulrich, and T. Wilpert, *Z. Phys. A* **322**, 241 (1985).
- [45] H. G. Bohlen, M. R. Clover, G. Ingold, H. Lettau, and W. von Oertzen, *Z. Phys. A: At. Nucl.* **308**, 121 (1982).
- [46] M. Buenerd, A. Lounis, J. Chauvin, D. Lebrun, P. Martin, G. Duhamel, J. C. Gondrand, and P. DeSaintignon, *Nucl. Phys. A* **424**, 313 (1984).
- [47] M. P. Nicoli, F. Haas, R. M. Freeman, N. Aissaoui, C. Beck, A. Elanique, R. Nouicer, A. Morsad, S. Szilner, Z. Basrak, M. E. Brandan, and G. R. Satchler, *Phys. Rev. C* **60**, 064608 (1999).
- [48] Y. Sugiyama, Y. Tomita, H. Ikezoe, Y. Yamanouchi, K. Ideno, S. Hamada, T. Sugimitsu, M. Hijiya, and Y. Kondō, *Phys. Lett. B* **312**, 35 (1993).
- [49] E. Stiliaris *et al.*, *Phys. Lett. B* **223**, 291 (1989).
- [50] H. G. Bohlen, E. Stiliaris, B. Gebauer, W. von Oertzen, M. Wilpert, Th. Wilpert, A. Ostrowski, D. T. Khoa, A. S. Demyanova, and A. A. Ogloblin, *Z. Phys. A* **346**, 189 (1993).
- [51] G. Bartnitzky *et al.*, *Phys. Lett. B* **365**, 23 (1996).
- [52] J. C. Owen, R. F. Bishop, and J. M. Irvine, *Ann. Phys. (NY)* **102**, 170 (1976).
- [53] M. Modarres and J. M. Irvine, *J. Phys. G* **5**, 511 (1979).
- [54] M. Modarres and G. H. Bordbar, *Phys. Rev. C* **58**, 2781 (1998).
- [55] M. Modarres and J. M. Irvine, *J. Phys. G* **5**, L7 (1979).
- [56] G. H. Bordbar and M. Modarres, *Phys. Rev. C* **57**, 714 (1998).
- [57] M. Modarres, A. Rajabi, and H. R. Moshfegh, *Phys. Rev. C* **76**, 064311 (2007).
- [58] B. S. Pudliner, V. R. Pandharipande, J. Carlson, S. C. Pieper, and R. B. Wiringa, *Phys. Rev. C* **56**, 1720 (1997).
- [59] M. Modarres, A. Tafrihi, and A. Hatami, *Nucl. Phys. A* **879**, 1 (2012).
- [60] S. Fantoni and S. Rosati, *Lett. Nuovo Cimento* **16**, 531 (1976).
- [61] J. G. Zabolitzky, *Phys. Rev. A* **16**, 1258 (1977).
- [62] A. Sarsa, S. Fantoni, K. E. Schmidt, and F. Pederiva, *Phys. Rev. C* **68**, 024308 (2003).
- [63] A. Akmal, V. R. Pandharipande, and D. G. Ravenhall, *Phys. Rev. C* **58**, 1804 (1998).
- [64] R. B. Wiringa, V. Fiks, and A. Fabrocini, *Phys. Rev. C* **38**, 1010 (1988).
- [65] S. Gandolfi, A. Yu. Illarionov, K. E. Schmidt, F. Pederiva, and S. Fantoni, *Phys. Rev. C* **79**, 054005 (2009).